

JVN observations of H₂O masers around the evolved star IRAS 22480+6002

Hiroshi IMAI¹, Takahiro FUJII^{1,2}, Toshihiro OMODAKA¹
 and

Shuji DEGUCHI³

¹*Department of Physics, Faculty of Science,
 Kagoshima University, 1-21-35 Korimoto, Kagoshima 890-0065*

²*VERA Project Office, National Astronomical Observatory,
 2-21-1 Osawa, Mitaka, Tokyo 181-8588*

³*Nobeyama Radio Observatory, National Astronomical Observatory,
 Minamimaki, Minamisaku, Nagano 384-1305
 (HI: hiroimai@sci.kagoshima-u.ac.jp)*

(Received 2007 May 30; accepted 2007 September 18)

Abstract

We report on the H₂O maser distributions around IRAS 22480+6002 (=IRC+60370) observed with the Japanese VLBI Network (JVN) at three epochs spanning 2 months. This object was identified as a K-type supergiant in 1970s, which was unusual as a stellar maser source. The spectrum of H₂O masers consists of 5 peaks separated roughly equally by a few km s^{−1} each. The H₂O masers were spatially resolved into more than 15 features, which spread about 50 mas along the east–west direction. However, no correlation was found between the proper motion vectors and their spatial distributions; the velocity field of the envelope seems random. A statistical parallax method applied to the observed proper-motion data set gives a distance of 1.0 ± 0.4 kpc for this object, that is considerably smaller than previously thought. The distance indicates that this is an evolved star with $L \sim 5800 L_{\odot}$. This star shows radio, infrared, and optical characteristics quite similar to those of the population II post-AGB stars such as RV Tau variables.

Key words: masers — stars:mass loss — stars: supergiant — stars:individual (IRAS 22480+6002)

1. Introduction

H₂O maser emission has been observed in circumstellar envelopes of evolved stars such as O-rich Mira variables and OH/IR stars with large mass loss rates of $\dot{M} \geq 10^{-7} M_{\odot} \text{ yr}^{-1}$ (Reid & Moran 1981; Elitzur 1992). Most of these stars are asymptotic giant branch (AGB) stars or red supergiants both with the spectral type M, with a few exceptions for transient stars at pre-planetary nebula phase (or supposedly a few pre-main sequence stars such as Ori KL; Morino et al. 1998). For the central stars with spectral types earlier than M, UV radiation from stellar chromosphere eventually dissociates most of molecules (except CO) in the inner envelope (e.g., Wirsich 1998). Therefore, H₂O (or SiO) masers are usually not expected for these stars, except for the case that the molecules in dense circumstellar clumps shield themselves from UV radiation. In fact, H₂O masers found in a young planetary nebula (Miranda et al. 2001; Suárez et al. 2007) must be such an exceptional case. OH masers have been found in yellow hypergiants with spectral types F and G (such as IRC+10420 and V1427 Aql) (Giguere et al. 1976; Nedoluha & Bowers 1992; Humphreys et al. 2002). However, H₂O and SiO masers have never been detected in these objects (Nakashima & Deguchi 2003), though thermal emission of a few other molecules have been observed in the outer circumstellar shell (Castro-Carrizo et

al. 2001; Teyssier et al. 2006).

The optical counterpart of IRAS 22480+6002 (=AFGL 2968, or IRC+60370) was identified as a K-type supergiant (K0Ia; Humphreys & Ney 1974, or K4.5Ia; Fewley 1977). Therefore, the detections of H₂O and SiO masers (Han et al. 1998; Nyman et al. 1998) were surprising. Though a search for OH 1612 MHz emission was negative (Le Squeren et al. 1992), CO emission was detected toward this star (Josselin et al. 1998). From the CO $J = 2-1$ line profile, the systemic stellar velocity and the expansion velocity of this star were obtained to be $V_{\text{lsr}} = -49.3 \text{ km s}^{-1}$ and $V_{\text{exp}} = 26.4 \text{ km s}^{-1}$, respectively (Josselin et al. 1998; Groenewegen et al. 1999). They are consistent with those obtained from the H₂O and SiO maser spectra, and the expansion velocity of the envelope of this star is typical for OH/IR stars. The radial velocity gives a kinematic distance of 5.0 kpc. It suggests a large luminosity $L_{*} = 140\,000 L_{\odot}$ of the central star (Groenewegen et al. 1999), but it is consistent with the supergiant interpretation of this object. A blue nearby star, a B5II star, is seen by about 12'' east of this object. Though it is cataloged as a visual binary (Worley & Douglass 1997), a physical association of this object with the maser source is questionable because of the large velocity difference of about 40

Table 1. Status of the telescopes, data reduction, and resulting performances in the individual epochs of the JVN observations.

Observation code	Epoch in the year 2005	Duration (hr)	Used telescopes ¹	Reference velocity ² (km s ⁻¹)	1- σ level noise (Jy beam ⁻¹)	Synthesized beam ³ (mas)	Number of detected features
r05084b ...	March 25	7.3	MZ, IR, OG, IS, KS, NB ⁴	-52.3	0.22	1.7×1.6, -37°	20
r05116b ...	April 26	7.3	MZ, IR, OG, IS ⁵ , KS, NB	-52.0	0.15	3.8×2.0, -14°	17
r05151a ...	May 31	8.1	MZ, OG ⁵ , IS ⁵ , KS, NB	-52.6	0.15	3.2×2.8, -66°	14

¹ Telescopes that were effectively operated and whose recorded data were valid: MZ: the VERA 20 m telescope at Mizusawa, IR: the VERA 20 m telescope at Iriki, OG: the VERA 20 m telescope at Ogasawara Is., IS: the VERA 20 m telescope at Ishigakijima Is., KS: the NiCT 34-m telescope at Kashima, NB: the NRO 45-m telescope at Nobeyama.

² Velocity channel used for the phase reference in data reduction.

³ The synthesized beam made in natural weight; major and minor axis lengths and position angle.

⁴ Ceasing operation for 2.5 hr due to strong winds and pointing correction.

⁵ High system temperature (>300 K) due to bad weather conditions.

km s⁻¹ (Humphreys & Ney 1974). Winfrey et al. (1994) gave a new spectral classification of M0I for IRAS 22480+6002 from the low-resolution spectrum between 6000 and 8800 Å, which was significantly different from the previous type assignment of this star. For a long-period variable, optical spectral classification may vary with light variations. However, this star has not been reported as a variable star, though it is optically not very faint ($V \sim 8.3$).

In this work, we report three-epoch VLBI observations of H₂O masers of IRAS 22480+6002 to rectify the entangled situation associated with this object. From the spatio-kinematics of the masers, we diagnose a probable anomaly of a hot wind from the K-type star. We estimated the distance to this star using the statistical parallax method based on the proper motion data of H₂O masers. Our result gives a much smaller distance for this star than previously thought. The new estimation of the distance demands to reconsider various properties of this star. Based on the arguments presented in section 3, we conclude that this star is a population II post-AGB star.

2. Observations and Data Reduction

The 22 GHz VLBI observations were made at three epochs during 2005 March–May, using six telescopes of the Japanese VLBI Network¹. Table 1 gives a summary of status of the observations. At each epoch, the observation was made for ~ 7.5 hours including scans at the object and the calibrator (J2202+4216). The signal was recorded with a rate of 128 Mbit s⁻¹ and in two baseband channels with a band width of 16 MHz each. The VERA telescopes also simultaneously observed the position reference source J2254+6209 with the object using the dual beam system (e.g., Honma et al. 2003), but the reference source was not detected.

The data reduction, and identification of maser spots and features were made using the NRAO AIPS package

in the same setup and procedures as those described in Imai et al. (2006) and Inomata et al. (2007). The spectral channel spacing was set to 0.21 km s⁻¹. A typical size of the synthesized beam was 2.5 milliarcseconds (mas) in the three observations (see Table 1). A relative position accuracy of a maser spot (a component which appears in a single velocity channel) was typically 0.05 mas depending on a signal-to-noise ratio and spatial structure of the spot. A relative position accuracy of a maser feature (a cluster of maser spots which compose a physical clump) was typically 0.15 mas. Relative proper motions were measured for maser features, which were identified at least at two of the three epochs. Table 2 gives a list of relative positions of these maser features, their proper motions, radial velocities, and peak intensities.

Using the fringe-rate mapping method, we estimated the absolute coordinates of the maser feature IRAS 22480+6002: I2007 2 (the $V_{\text{lsr}} = -58.48$ km s⁻¹ component) to be R.A.(J2000.0)=22^h49^m58^s.876, and decl.(J2000.0)=+60°17′56″.65, with uncertainty of $\sim 0''.1$. The feature location is coincident with the 2MASS position of the bright star J22495897+6017568, or with the GSC 2.2 position of N012302336407, within 0.8'' and 0.6'', respectively.

3. Results and discussion

3.1. Spatial distribution and proper motions of maser features

Figure 1 shows cross-power spectra of the H₂O masers of IRAS 22480+6002. The H₂O maser emission spread in a velocity range of 15 km s⁻¹, which is typical for Mira-type AGB stars (e.g., Takaba et al. 1994). Five spectral peaks were seen in roughly equal separations of 2–3 km s⁻¹; the second highest peak was near the systemic velocity ($V_{\text{lsr}} = -49.3$ km s⁻¹). The correlated powers of these peaks equally increased by a factor of two during 2 months in our observing run, except for the second peak for which the intensity increased only by about 20%. However, the peak flux densities of individual features were found not to vary much (Table 2). This fact indicates that extended emissions were partially resolved in the shortest baseline between NRO and NICT (197.4 km), but resolved-out in

¹ JVN involves the NRO 45-m telescope at Nobeyama, the NiCT 34-m telescope at Kashima, and 4 VERA 20-m telescopes. NRO and VERA observatories are branches of the National Astronomical Observatory of Japan, a member institute of the inter-university research agency, NINS.

Table 2. Parameters of the H₂O maser features identified by proper motion toward IRAS 22480+6002.

Feature ¹	Offset (mas)		Proper motion ² (mas yr ⁻¹)				Radial motion ³ (km s ⁻¹)		Peak intensity at 3 epochs (Jy beam ⁻¹)		
	Δ R.A.	Δ decl.	μ_x	$\sigma(\mu_x)$	μ_y	$\sigma(\mu_y)$	V_z	ΔV_z ⁴	Epoch 1	Epoch 2	Epoch 3
1	-6.56	-10.69	4.20	1.46	5.86	1.40	-59.78	0.26	0.19	0.17	...
2	0.00	0.00	0.00	0.36	0.00	1.29	-58.48	2.74	2.33	2.72	3.48
3	-45.23	7.26	-0.87	0.42	0.51	0.66	-55.01	2.04	3.77	2.47	2.42
4	-4.95	7.17	0.25	0.29	0.47	1.44	-54.33	1.05	0.41	0.53	0.73
5	-26.70	-2.86	-1.03	0.97	-0.72	0.61	-52.34	3.37	8.11	8.73	8.16
6	-0.37	1.50	3.96	1.29	0.86	1.91	-50.37	0.56	0.53	0.73	0.49
7	0.16	2.74	0.05	0.61	0.98	1.56	-49.29	2.18	8.44	7.96	6.20
8	-0.04	13.96	0.90	0.67	-0.29	0.78	-47.88	1.33	1.92	1.69	1.03
9	-34.92	-7.63	-1.95	1.66	-3.07	2.97	-47.39	0.52	0.25	0.26	...
10	-48.23	11.08	2.27	1.18	0.71	0.88	-47.24	0.56	0.24	0.20	0.18
11	-2.24	8.18	0.06	1.10	-0.16	0.64	-46.17	0.84	0.41	0.28	0.26
12	-1.02	13.29	0.06	0.41	0.56	0.74	-45.37	1.97	3.34	3.40	2.44
13	0.13	7.77	-1.86	3.19	0.26	1.32	-44.40	0.77	0.24	0.33	0.32

¹ H₂O maser features detected toward IRAS 22480+6002. The feature is designated as IRAS 22480+6002:I2007 *N*, where *N* is the ordinal source number given in this column (I2007 stands for sources found by Imai et al. and listed in 2007).

² Relative value with respect to the motion of the position-reference maser feature: IRAS 22480+6002:I2007 2.

³ Relative value with respect to the local stand of rest.

⁴ Mean full velocity width of a maser feature at half intensity.



Fig. 1. Cross-power spectra of H₂O masers in IRAS 22480+6002 obtained in the baseline between the NRO 45m and NICT 34m telescopes at three epochs.

the longer baselines. Correlated flux densities were estimated to be about 30–40% of the total-power intensities. Figure 2 shows the distribution of maser features at the first epoch. The extent of 50 mas corresponds to 50 AU ($D/1$ kpc), which is somewhat larger than those seen around Mira variables at $D = 1$ kpc (e.g., Bowers & Johnston 1994). In this figure, one of the low-velocity (blue-shifted) components ($V_{\text{lsr}} = -58.48$ km s⁻¹; the position reference) is located at the origin and the other low velocity components (in grey and blue colors) are located both near the eastern and western edges. Many of the

higher velocity (red-shifted) components (shown in yellow, orange, and red colors) fall at the eastern edge, but a few of them are scattered at the west side too. The overall distribution of water maser features are characterized by the elongation to the east-west direction. But, no clear correlation is found between the velocities and spatial positions. If the circumstellar envelope of the K supergiant interacts with the wind from the eastern BII star (though this is unlikely), maser spots and features could be aligned perpendicularly to the wind direction, i.e., in the north-south direction (e.g., Imai et al. 2002). We find no such N-S alignment of the H₂O maser features. Meixner et al. (1999) noted that the MIR image of this star with the NASA 3-m telescope showed a northeast-southwest elongation, but concluded that it was likely to be an artifact caused by astigmatism.

We detected 14–20 H₂O maser features though all epochs (the last column of table 1). Note that the H₂O masers were persistent in velocity and in spatial distribution during the two months; 65–90% of the detected maser features survived during our observing run. Therefore, we identified the same maser features at three epochs relatively easily, and measured the proper motions of the individual features during two months. Table 2 gives the measured proper motions. Figure 3 shows the linear fits to the relative positions of the individual maser features. The fitted proper motions look significant with the second epoch contributing little for most features, which warrants our selecting the same maser features at the different epochs. Circumstellar H₂O masers can amplify the radiation of the central star (for example, see the case of U



Fig. 2. Distribution of H₂O masers on 2005 March 25. The color code indicates the radial velocity of the feature, and the size of the filled circle indicates the flux density of the feature. Note that the -58.48 km s^{-1} reference component is located at the origin (light blue), but is almost overlapped with the systemic-velocity component ($\sim -49 \text{ km s}^{-1}$) shown in green.

Her; Vlemmings et al. 2002). In the present case, we may speculate that the -52.34 km s^{-1} feature (No. 5 in Table 2 and Figure 4), which is one of the strongest components and located near the center of the maser distribution, is such a maser amplifying the stellar radiation. However, it is hasty to draw any conclusion from this observation, since we have no information on the central-star position in this scale.

Figure 4 shows the proper motion vectors of the individual H₂O maser features. Note that the largest two proper-motion vectors at the lower left and lower right, i.e., features 1 and 9 of the $V_{\text{lsr}} = -59.78$ and -47.39 km s^{-1} components, respectively, were determined by two-epoch detections, so that they are slightly inaccurate. The proper motions of all other features with 3-epoch detections are within a few mas per year (relative to the reference component at $V_{\text{lsr}} = -58.48 \text{ km s}^{-1}$). We cannot find any systematic trend of motions in this diagram. For example, features 3 and 10 at the western edge move in opposite directions, and features 6 and 13 at the eastern edge also move in opposite directions.

Figure 5 shows the RA-offsets and μ_x plots against V_{lsr} . The ellipse is a plot of expected offset and proper motion from a thin spherical-shell model with a constant velocity (in the Right Ascension direction because the maser features are spread mainly in this direction). If the shell model is correct, all of the maser features should fall between these ellipses. However, the right panel does not show such a tendency. Rather, the observed points seem to distribute randomly.

The randomness of the proper motions may partially

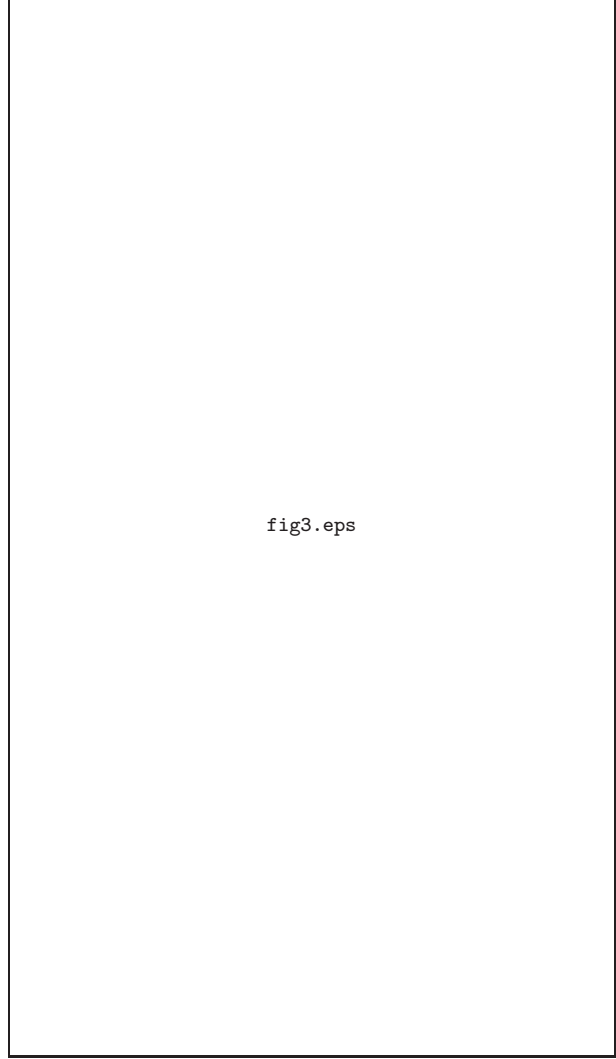


Fig. 3. Observed relative proper motions of H₂O maser features in IRAS 22480+6002 in R.A. (a) and decl. (b) directions. The number on the left indicates the feature name designated in Table 2. The vertical bar attached to each data point indicates the position uncertainty. The least-square-fitted line is also shown.

originate from the large random errors in the position measurements. In order to check this issue, we made a Monte Carlo simulation of the 3-epoch proper motion fitting with the same positional uncertainties but without real motions (i.e., position jitters only due to the measurement errors). We obtained the mean velocity dispersions ($0.79 \pm 0.25 \text{ mas yr}^{-1}$, $0.80 \pm 0.20 \text{ mas yr}^{-1}$) for the 13 proper motions in R.A. and Dec. directions for the present case from the simulations; here, the number after the ‘ \pm ’ sign is a standard deviation of dispersions obtained in the simulations. The observed velocity dispersions (1.95 mas yr^{-1} , 1.93 mas yr^{-1}), are significantly larger than the simulated mean dispersions (more than 4σ). Therefore, the observed proper motions are substantially real motions of masing features.

The observed random motions may originate from the intrinsic random ballistic motions of matters ejected from



Fig. 4. Doppler velocities (colorfully displayed) and relative proper motion vectors (indicated by arrows) of H₂O masers in IRAS 22480+6002. The displayed proper motion vector is that subtracted by a velocity bias $(\overline{\mu_x}, \overline{\mu_y}) = (0.97, 0.72)$ [mas yr⁻¹] from the original vector to cancel out the average motions of all the features. A number added for each feature with a proper motion shows the assigned one after the designated name form “IRAS 22480+6002: I2007”. The map origin is set to the location of the feature IRAS 22480+6002: I2007 2.

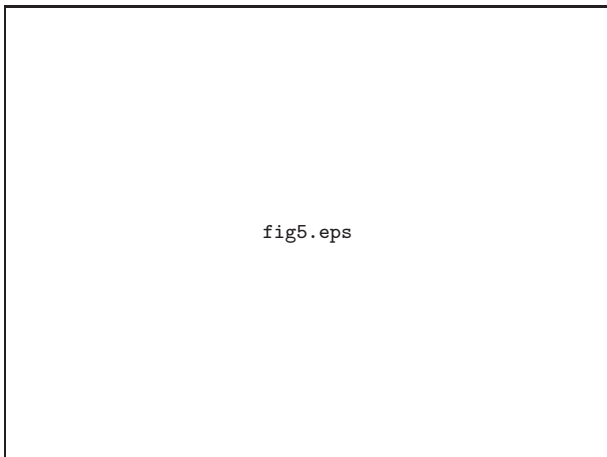


Fig. 5. Plot of relative R.A. offset (left) and proper motion (right) against radial velocity. The filled and unfilled circles indicate the three-epoch and two-epoch detections. The large and small ellipses in both panels indicate the position and proper motion curves expected from thin spherical shell models (one-dimensional in the R.A. direction) with a constant expansion velocity of 12.5 km s⁻¹ and a radius of 3.5×10^{14} cm, and with 7 km s⁻¹ and 8×10^{13} cm, respectively both at a distance of 0.9 kpc. The observed points in the right panel do not fit to these ellipses.

or infalling into the atmosphere of the central supergiant. This may be a characteristic of mass outflow of a supergiant originating from the extended atmosphere which is considerably turbulent (Levesque et al. 2005; Josselin & Plez 2007). The motion of 1 mas yr⁻¹ corresponds a transverse motion of $\sim 4.7(D/\text{kpc})$ km s⁻¹. In order to obtain the distance, we applied the statistical parallax method to the obtained maser proper motions; for exam-

ple, see Schneps et al. (1981). Assuming random motions of maser features, we obtained a velocity dispersion in radial motion (with respect to the average velocity of maser features, $V_{\text{lsr}} = -50.6$ km s⁻¹) to be $\sigma_v \simeq 5.0$ km s⁻¹, which is smaller than the outflow velocity estimated from CO emission.

The dispersion in the maser proper motions can be obtained by subtracting the dispersion involved in the measurements; see equation (3) of Schneps et al. (1981). We obtain $\sigma_\mu \sim 1.40$ mas yr⁻¹ and get a distance to IRAS 22480+6002 to be $D = \sigma_v / \sigma_\mu = 0.76 (\pm 0.25)$ kpc. The formal uncertainty involved in the distance estimation was computed using equation (4) of Schneps et al. (1981). If we exclude the largest two proper-motion features with two-epoch detections from the sample, we get the distance $1.02 (\pm 0.38)$ kpc. Later on, we adopt this distance for IRAS 22480+6000, because large motions detected by two-epoch observations are somewhat dubious. Note that this distance is derived based on the assumption that the velocity field of masers is random and isotropic, and that the proper motions appeared in maser features are real motions of gas clumps. The distance 1.0 kpc gives a radius of water maser shell approximately 3.7×10^{14} cm, which is compatible with the radii of water maser shells of miras, but considerably smaller than those of M-supergiants (Yates & Cohen 1994; Cotton et al. 2004). Though the obtained distance still involve a considerable uncertainty, it excludes the possibility of a very large distance of 5 kpc (a kinematic distance).

The luminosity of this star is re-evaluated to be $5.8 \times 10^3 L_\odot$ (reestimated from Groenewegen et al. 1999). It is considerably small for a supergiant. However, from the distance of 1.0 kpc, we can compute the absolute V magnitude of this star from 2MASS K magnitude ($K = 2.8$) using $V - K = 3.7$ (for K5III; Zombeck 1990), and with reddening corrections, we get $M_V \sim -4.4$. This value falls near the absolute magnitude of K5Ib (or M0Ib) (Zombeck 1990). Therefore, the luminosity is still in a range of supergiants.

The radial velocity of ~ -50 km s⁻¹ is typical for young objects in the Perseus spiral arm in the direction of this star (for example, see Sitnik 2003). If we take into account the large uncertainties involved in the obtained distance, we cannot completely exclude the possibility that IRAS 22480+6002 belongs to the Perseus arm at $D \sim 3.0$ kpc at $l = 108^\circ$ (Xu et al. 2006). However, there are several other bright stellar maser sources with similar radial velocities in the same direction, e.g., CU Cep (-50 km s⁻¹), IRC+60374 (-52 km s⁻¹), and AFGL 2999 (-50 km s⁻¹). Luminosity distances to these stars are inferred to be smaller than 3 kpc from their high IRAS flux densities. In addition, MY Cep is an M supergiant with $V_{\text{lsr}} = -56$ km s⁻¹ in the star cluster NGC 7419. The distance to this cluster has been well estimated to be about 2.3 kpc from luminosities of member stars of the cluster (e.g., see Beauchamp et al. 1994; Subramaniam et al. 2006). These example indicates that the stars with $V_{\text{lsr}} \sim -50$ km s⁻¹ do not necessarily belong to the Perseus arm, but they may be located much closely. Because the radial veloc-

ity expected by the galactic rotation is only ~ -10 km s $^{-1}$ at 1 kpc at $l = 108^\circ$, and because the radial-velocity dispersion of stellar maser sources is as small as ~ 25 km s $^{-1}$ at the solar neighborhood (see Appendix 2 of Deguchi et al. 2005), IRAS 22480+6002 is possibly kinematically anomalous.

3.2. Past optical/infrared data of IRAS 22480+6002 (=J22495897+6017568).

Though this star is relatively bright at optical wavelengths ($V \sim 8.30$; Tycho Input catalog), the star was not recorded in major optical catalogs, for example, not in Henry Draper (HD) Catalogue, The Hipparcos and Tycho Catalogue, nor the General Catalog of Variable Stars, possibly because of confusion by the nearby B5II star (TYC 4265-870-1; $V \sim 10.74$), located by about $12''$ east. This was involved in The Washington Double Star Catalog², giving a separation of $10.9''$ in 1901 and $12.0''$ in 2006 with a small position angle variation (by $\sim 7^\circ$) to the B star. From this data, we obtain the proper motion of 17 mas yr $^{-1}$ to the west for IRAS 22480+6002 relative to this B star. As noted by Humphreys & Ney (1974), this B5II star is probably not a binary counterpart because of the large radial velocity difference. The ACT Reference Catalog gave a very small proper motion of this B5II star (less than 3 mas yr $^{-1}$); though The Hipparcos and Tycho Catalogue gave a large proper motion in declination due to position uncertainty, but this was corrected in ACT catalog. We also checked the past catalogs recording the position of this star and summarized the results in table 3.³ The GSC 1.2 catalog (which remeasured the POSS1 plate taken in 1950s) gave a different position by about $4.2''$, which leads a large proper motion of 84 mas yr $^{-1}$ if compared with GSC 2.0. This value is much larger than the above-mentioned proper motion computed from the Washington Double Star Catalog, though the proper motion vectors are roughly in the same direction. We believe the direct measurements of binary separation gives better values. Therefore, we adopt the proper motion of 17 mas yr $^{-1}$ for this star, and get $U_0 = -71$ km s $^{-1}$ and $V_0 = -29$ km s $^{-1}$ for IRAS 22480+6002. This motion is considerably peculiar for a population I disk star. It is likely that IRAS 22480+6002 belongs to one of kinematical streaming groups of stars as population II G and K giants (Famaey et al. 2005).

In the past, OH and H₂O masers have been found in a few planetary and preplanetary nebulae (Zijlstra et al. 1989; Miranda et al. 2001; Suárez et al. 2007), where central stars of these objects have spectral types earlier than M. These masers are a remnant of circumstellar material which was ejected at the AGB phase of the central star. The molecules responsible for masers are eventually to be dissociated. In contrast, Fix & Claussen (1984) found OH 1665/1667 MHz emission toward several warm stars as RV Tau variables with spectral type of G and K, but so far only one case (TW Aql, a semi-regular variable of K7III)

was confirmed to be a circumstellar maser (Planesas et al. 1991). SiO masers, which are emitted within a few stellar radii of the central star (much closer than H₂O masers are emitted), were not detected in these warm objects before. An exceptional case is the RV Tau variable, R Sct, with spectral type K0Ib. This object exhibits strong SiO and weak H₂O masers (I. Yamamura, 2004 private communication) as well as the $4 \mu\text{m}$ SiO first overtone bands (Matsuura et al. 2002). The RV Tau variables are believed to be low-mass post-AGB stars (Jura et al. 1986) with low metal abundances (population II; Gridhar et al. 1999), though these are spectroscopically classified as supergiants. Their spectral types change between K and M-type with light variation (Pollard et al. 1997). The atmosphere of late-type supergiants are not in hydrostatic equilibrium; effective temperature increases with decreasing metallicity (Levesque et al. 2005). The RV Tau variables are enshrouded by dust shell, and CO emission has been detected in two of these variables (Bujarrabal et al. 1988). Although the optical counterpart of IRAS 22480+6002 is not reported to show any strong light variability (e.g., TASS; The Amateur Sky Survey⁴), the optical spectroscopic classification, middle infrared properties, and maser characteristics of IRAS 22480+6002 indicate a close similarity to the properties of the RV Tau variables.

4. Summary

We observed the H₂O maser emission distribution around the evolved star IRAS 22480+6002 with the Japanese VLBI Network. The maser emission was found to come from an area elongated in the east-west direction by about 50 mas, but no clear trend was found between radial velocities and spatial positions. With the three-epoch two-month interval VLBI observations, we found relatively large proper motions of a few up to 5 mas yr $^{-1}$ for individual H₂O maser features. They exhibit no systematic trend in their velocity field, and the inner envelope of this star is very disturbed. Applying the statistical parallax method, we obtained a distance of $\sim 1.0 \pm 0.4$ kpc, which is significantly smaller than the value previously thought. This distance gives a small luminosity of $\sim 6 \times 10^3 L_\odot$, but not unreasonably small as a K5 or M0-type supergiant. Combination of the distance and the previous optical proper motion data of this star place this object to be in a dynamically streaming group of stars. The maser characteristic, and optical and infrared properties of this star are quite similar to those of population II post-AGB stars as RV Tau variables.

We acknowledge all staff members and students who have helped in array operation and in data correlation of the JVN/VERA. H. I. was supported by Grant-in-Aid for Scientific Research from Japan Society for Promotion Science (18740109). This research was made use of VizieR database, operated at CDS, Strasbourg, France.

² available at <http://ad.usno.navy.mil/wds/wdtext.html>.

³ all the data except JVN are available in the VizieR database (<http://vizier.nao.ac.jp/viz-bin/VizieR>).

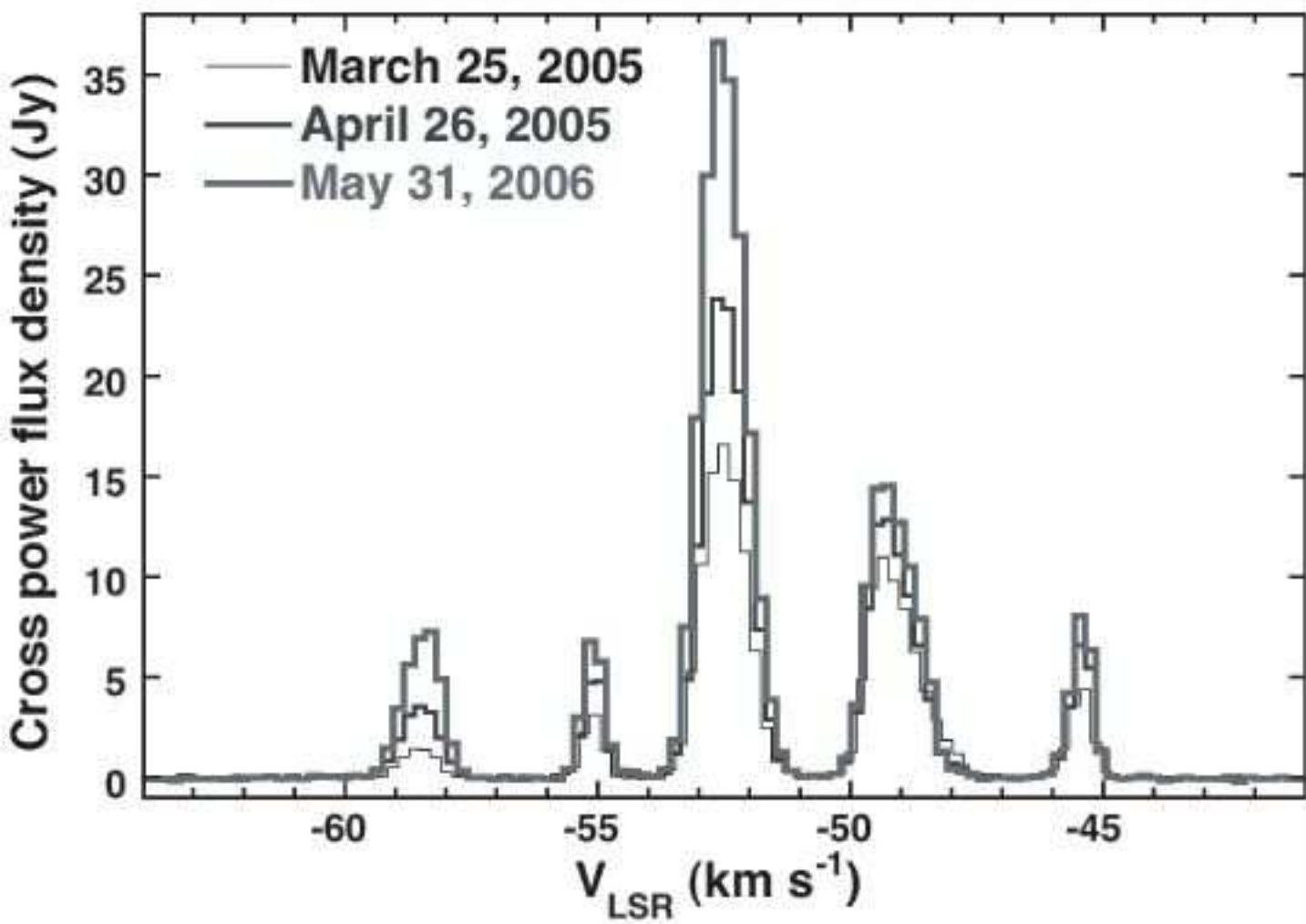
⁴ data available at <http://www.tass-survey.org/>

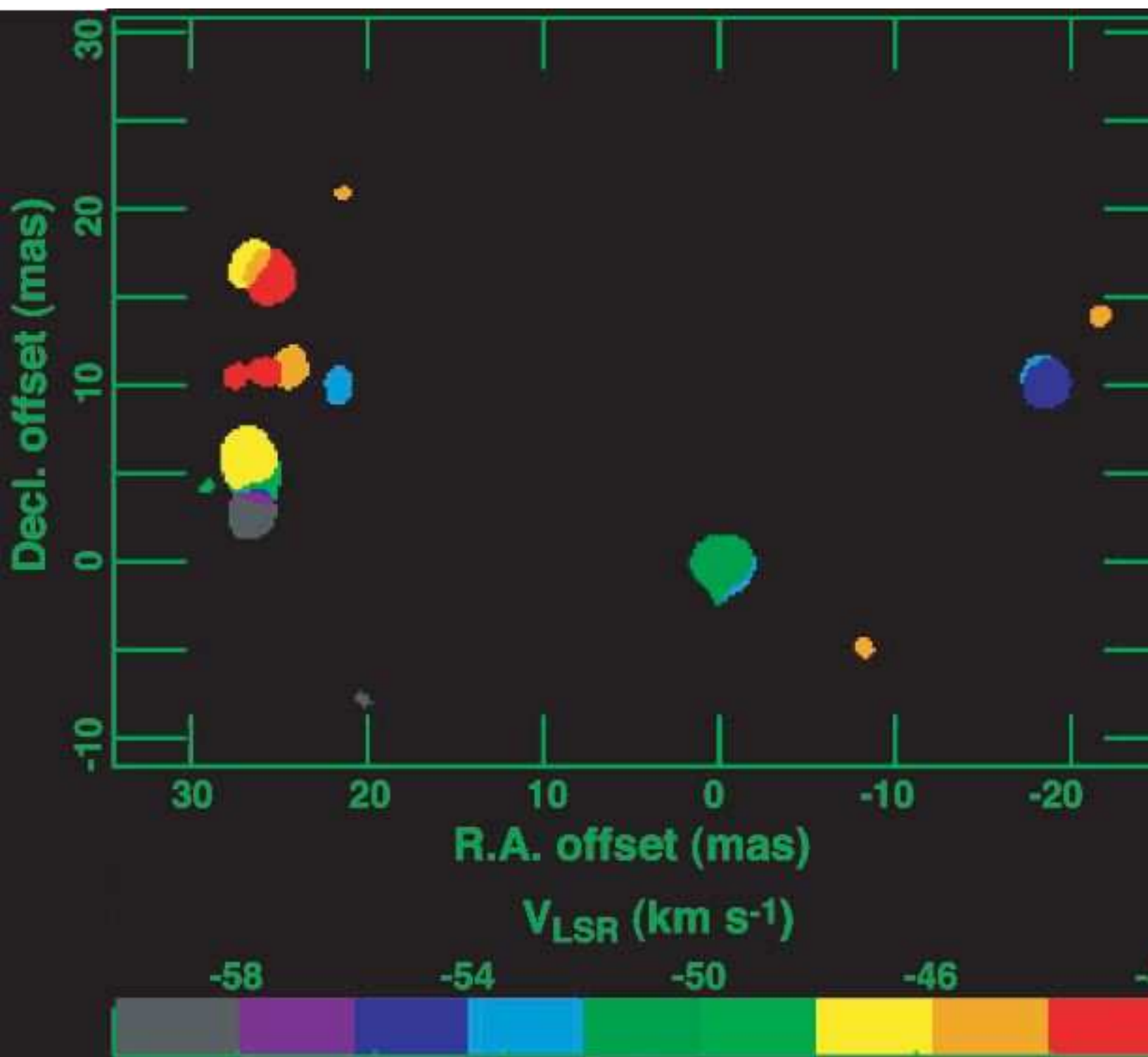
Table 3. Comparison of the catalogued positions of IRAS 22480+6002.

Catalog	Band	Assignment	epoch	R.A.(J2000) h m s	decl.(J2000) ° ' "	error "	flux density or magnitude
IRAS	MIR	22480+6002	1983	22 49 59.2	+60 17 55	$11'' \times 5''$ (19°)	$F_{12} = 142$ Jy
MSX6	MIR	G108.4255+00.8939	1995	22 49 58.89	+60 17 56.8	0.3	$F_C = 123$ Jy
2MASS	NIR	2495897+6017567	1997	22 49 58.97	+60 17 56.8	0.29	K=2.78
GSC1.2	optical	0426500695	1954	22 49 59.43	+60 17 55.8	0.3	R=12.29
GSC2.2	optical	N012302336407	1989.6	22 49 58.900	+60 17 57.17	0.3	B=12.29
USNO-B1.0	optical	1502-0356025	1971.7	22 49 59.75	+60 17 56.7	(0.7, 1.0)	R=8.87
USNO-B1.0	optical	1502-0356023	1979.7	22 49 59.44	+60 17 55.9	(0.7, 0.2)	R=8.73
USNO-B1.0	optical	1502-0356019	1979.7	22 49 59.15	+60 17 57.5	(0.5, 0.7)	B=12.63
JVN (this work)	radio	22480+6002	2005.5	22 49 58.876	+60 17 56.65	0.1''	$F_{H_2O} \sim 8$ Jy

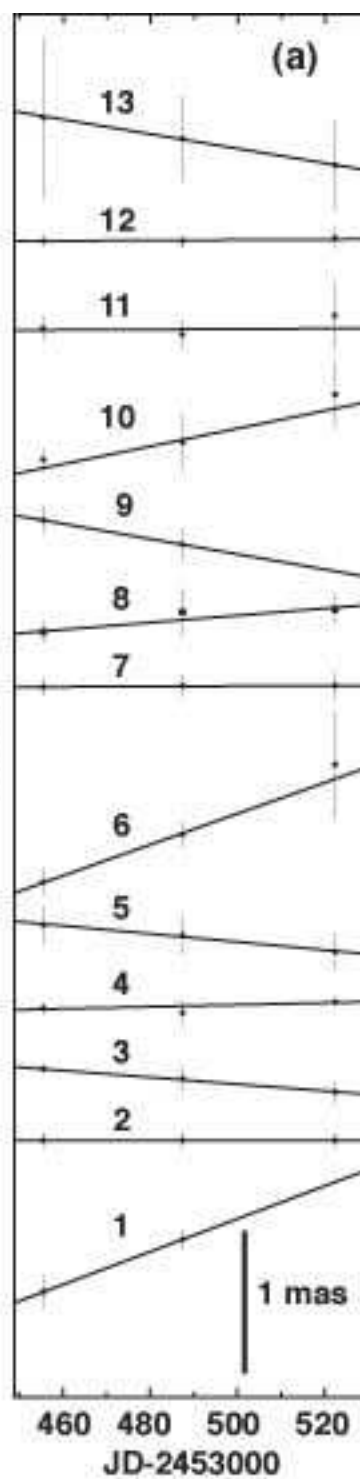
References

- Beauchamp, A., Moffat, A. F. J. & Drissen, L. ApJS, 93, 187
Bowers, P. F., & Johnston, K. J. 1994, ApJS, 92, 189
Bujarrabal, V., Bachiller, R., Alcolea, J., & Martin-Pintado, J. 1988, A&A, 206, L17
Castro-Carrizo, A., Lucas, R., Bujarrabal, V., Colomer, F., & Alcolea, J. 2001, A&A368, L34
Cotton, W. D., Mennesson, B., Diamond, P. J., Perrin, G., Coudé du Foresto, V., et al. 2004, A&A, 414, 275
Deguchi, S., Nakashima, J., Miyata, T., & Ita, Y. 2005, PASJ, 57, 933
Elitzur, M. 1992, in *Astronomical Masers* (Dordrecht: Kluwer)
Fewley, W. M. 1977, ApJ, 218, 181
Famaey, B., Jorissen, A., Luri, X., Mayor, M., Udry, S., Dejonghe, H., & Turon, C. 2005, A&A, 430, 165
Fix, J. D., & Claussen, M. J. 1984, ApJL, 287, L3
Giguere, P. T., Woolf, N. J., & Webber, J. C. 1976, ApJ207, L195
Giridhar, S., Lambert, D. L., & Gonzalez, G., 2000, ApJ., 531, 521
Gledhill, T. M., Yates, J. A., Richards, A. M. S. 2001, MNRAS, 328, 301,
Groenewegen, M. A. T., Baas, F., Blommaert, J. A. D. L., Stehle, R., Josselin, E., & Tilanus, R. P. J. 1999, A&AS, 140, 197
Han, F., et al. 1998, A&AS, 127, 181
Honma, M. et al. 2003, PASJ, 55, L57
Humphreys, R. M., & Ney, E. P. 1974, PASJ, 86, 444
Humphreys, R. M., Davidson, K., & Smith, N. 2002, AJ, 124, 1026
Imai, H., Omodaka, T., Hirota, T., Umemoto, T., Sorai, K., & Kondo, T. 2006, PASJ, 58, 883
Imai, H., Deguchi, S., & Sasao, T. 2002, ApJ, 567, 971
Imai, H., Obara, K., Diamond, P. J., Omodaka, T., & Sasao, T. 2002, Nature, 417, 829
Inomata, N., Imai, H., & Omodaka, T. 2007, PASJ(in press)
Josselin, E., Loup, C., Omont, A., Barnbaum, C., Nyman, L. A.; & Sevre, F. 1998, A&AS, 129, 45
Josselin, E. & Lèbre, A. 2001, A&A, 367, 826
Josselin, E. & Plez, B. 2007, A&A, 469, 671
Jura, M. 1986, ApJ, 309, 732
Le Squeren, A. M., Sivagnanam, P., Dennefeld, M., & David, P. 1992, A&A, 254, 133
Levesque, E. M., Massey, P., Olsen, K. A., & Plez, B. 2005, ApJ, 628, 973
Matsuura, M., Yamamura, I., Zijlstra, A. A., & Bedding, T. R. 2002, A&A, 387, 1022
Meixner, M., Ueta, T., Dayal, A., Hora, J. L., Fazio, G., Hrivnak, B. J., Skinner, C. J., Hoffmann, W. F., Deutsch, L. K., 1999, ApJS, 122, 221
Miranda, L. F., Gómez, Y., Anglada, G., & Torrelles, J. M. 2001, Nature, 414, 284
Morino, J., Yamashita, T., Hasegawa, T., & Nakano, T. 1998, Nature, 393, 340
Nakashima, J., & Deguchi, S. 2003, PASJ, 55, 229
Nedoluha, G. E. & Bowers, P. F. 1992, ApJ, 399, 743
Nyman, L.-Å., Hall, P. J., & Olofsson, H. 1998, A&AS, 127, 185
Planesas, P., Bujarrabal, V., Le Squeren, A. M., & Mirabel, I. F. 1991, A&A, 251, 133
Pollard, K. R., Cottrell, P. L., Lawson, W. A., Albrow, M. D. & Tobin, W. 1997, MNRAS, 286, 1
Reid, M., & Moran, J. 1981, ARA&A, 19, 231
Schneps, M. H., Moran, J. M., Genzel, R., Reid, M. J., Lane, A. P. & Downes, D. 1981 ApJ, 249, 124
Sitnik, T. G. 2003, Astr. Letter 29, 311
Subramaniam, A., Mathew, B., Bhatt, B. C., Ramya, S. 2006, MNRAS, 370, 743
Suárez, O., Gómez, J. F., Morata, O. 2007, A&A, 467, 1085
Takaba, H., Ukita, N., Miyaji, T., & Miyoshi, M. 1994, PASJ, 46, 629
Te Lintel Hekkert, P. T. L., Chapman, J. M., & Zijlstra, A. A. 1992, ApJ, 390, L23
Teyssier, D., Hernandez, R., Bujarrabal, V., Yoshida, H., & Phillips, T. G. 2006, A&A, 450, 167
Vlemmings, W. H. T., van Langevelde, H. J., & Diamond, P. J. 2002, A&A, 393, L33
Winfrey, S., Barnbaum, C., Morris, M., & Omont, A. 1994, BAAS, 185, 4515
Wirsich, J. 1998, ApJ, 502, 909
Worley, C.E., & Douglass, G.G. 1997, A&AS 125, 523
Xu, Y., Reid, M. J., Zheng, X. W., & Menten, K. M. 2006, Science, 311, 54
Yates, J. A. & Cohen, R. J. 1994, MNRAS, 270, 958
Zijlstra, A. A., Te Lintel Hekkert, P., Pottasch, S. R., Caswell, J. L., Ratag, M., & Habing, H. J. 1989, A&A, 217, 157
Zombeck, M. V. 1990, *Handbook of Space Astronomy and Astropysics*, 2nd ed. (New York; Cambridge Univ. Press), P71





Relative R.A. offset



Relative decl. offset



